Exploring exchange mechanisms with a cold-atom gas

P. O. Bugnion and G. J. Conduit

Cavendish Laboratory, J. J. Thomson Avenue, Cambridge CB3 0HE, United Kingdom

Fermionic atoms trapped in a double-well potential are an ideal setting to study fundamental exchange mechanisms. We use exact diagonalization and complementary analytic calculations to demonstrate that two trapped fermions deliver a minimal model of the direct-exchange mechanism. This is an ideal quantum simulator of the Heisenberg antiferromagnet, exposes the competition between covalent and ionic bonding, and can create, manipulate, and detect quantum entanglement. Three trapped atoms form a faithful simulator of the double-exchange mechanism that is the fundamental building block behind many Heisenberg ferromagnets.

Recent experimental advances allow investigators to confine up to ten atoms in a trap and address their quantum state [1,2]. This innovation enables the Heidelberg group to isolate two distinguishable fermions in a one-dimensional well and tune the interaction strength to induce fermionization [3], presenting a unique opportunity to study the fundamental physics of short-range repulsion [4–11]. This could allow experimentalists to realize an analog to the Stoner model for itinerant ferromagnetism [12,13]. However, many real-life solids are best described by spins that are localized in real space. These are commonly described by the Heisenberg model that predicts the direct- and double-exchange mechanisms behind the emergence of antiferromagnetism and ferromagnetism, respectively. Here we take advantage of the ability of the Heidelberg group to trap either two or three fermions in the double well potential to realize the first exact quantum simulators for the direct-exchange and double-exchange mechanisms. This allows us to not only study the minimal building block of Heisenberg magnetism but also build a quantum simulator to expose the competition between covalent and ionic bonding, and study quantum entanglement manipulation and detection.

The direct-exchange mechanism has previously been realized in double quantum dot systems [14–17] and cold-atom gases in an array of double-well potentials [18–20]. We now exploit the experimental flexibility of the Heidelberg group to isolate just two atoms and expose the phase behavior. We use exact diagonalization to deliver the full energy spectrum and a perturbative approach to gain an intuitive understanding of the phase behavior. The flexibility of the setup allows us to build the first quantum model of the fundamental covalent and ionic bonding mechanisms in molecules and crystals, allowing us to address the long-standing question of their relative contributions to chemical bonds [21]. A thorough understanding of the exchange energy also allows us to define a new protocol to create, control, and detect quantum entanglement [22,23].

The isolated double-exchange mechanism has not yet been realized experimentally. A faithful quantum simulator of the double-exchange mechanism is not only important for understanding Heisenberg ferromagnets but also describes the 90° superexchange mechanism and can be extended to larger systems through a quantum virial or cluster expansion [24,25]. Through exact diagonalization and a complementary perturbative analysis we demonstrate how the cold-atom gas

will probe the double-exchange mechanism with changing barrier height, interaction strength, and the ellipticity of the external trapping potential. This modifies the degeneracy of the ground state leading to a quantum phase transition that we expose with a statistical tunneling probe.

I. FORMALISM

We start from two-component Fermionic atoms with each species indexed by a pseudospin $\sigma \in \{\uparrow, \downarrow\}$. The atoms are trapped by an external harmonic potential with Hamiltonian $\hat{H} = -\nabla^2/2 + [\omega_\perp^2(x^2 + y^2) + \omega_\parallel^2 z^2]/2 + V_B \exp(-\omega_B z^2) + g(\mathbf{r}_\uparrow - \mathbf{r}_\downarrow)\hat{n}_\uparrow(\mathbf{r}_\uparrow)\hat{n}_\downarrow(\mathbf{r}_\downarrow)$, setting $\hbar = m = 1$ throughout. The parabolic trapping potential has a variable ellipticity that we associate with a length scale $a_\parallel = 1/\sqrt{\omega_\parallel}$. The Gaussian barrier $V_B \exp(-\omega_B z^2)$ will split the system into two wells. Throughout this paper we set its width with $\omega_B = 5\omega_\parallel$. We use two complementary techniques to analyze the system: (i) exact diagonalization to expose the full energy spectrum, and (ii) perturbation theory to deliver an intuitive description.

In exact diagonalization [26], we work in the eigenbasis of the noninteracting Hamiltonian. We express the orbitals in this basis as linear combinations of the Gaussian-type orbitals (GTOs) [27] of the harmonic trapping potential without the central barrier. Labeling these GTOs by the standard quantum numbers $\{n_x, n_y, n_z\}$, we include $0 \leqslant (n_x, n_y) < 4$ and $0 \leqslant n_z < 50$. Including basis functions with higher n_z is necessary to capture the effect of the central barrier on the orbitals.

To calculate the orbitals of the noninteracting system including the central barrier we first evaluate the noninteracting Hamiltonian matrix in the GTO basis. The matrix elements of the central Gaussian barrier can be conveniently expressed in terms of hypergeometric functions [28]. Having calculated the Hamiltonian matrix, we diagonalize it to obtain a list of orbitals to use in the subsequent calculation that incorporates the effect of interactions.

We construct the 10 000 Slater determinants with the lowest noninteracting energy to use as the many-body basis for our exact diagonalization calculation. To include interactions we evaluate the four-center integrals in the basis of our orbitals and construct the Hamiltonian matrix using the Slater-Condon rules [26]. Finally, we diagonalize the matrix to find the ground and excited states of the system.

In a cold-atom gas the Feshbach resonance is used to tune a contact interaction strength $V(\mathbf{r})$ from the repulsive through to the attractive regime. To generate a positive scattering length for a potential with a small effective range we use the square-well potential $g(\mathbf{r}) = -g\theta(R - |\mathbf{r}|)$ with a radius $R = 0.4a_\parallel$. This is significantly less than the width of the central barrier $2/\sqrt{\omega_B} \approx 0.9a_\parallel$ so that atoms localized in adjacent wells will not interact, and moreover we ensured that the energy of the states converged in the limit $R \to 0$. The well depth g was tuned to generate a positive or negative scattering length $a = R[1 - \tan(R\sqrt{g})/R\sqrt{g}]$ and was constrained to $0 \leqslant R\sqrt{g} < 4.49$ to confine at most one bound state. However, the inclusion of the bound state leads to many molecular states crossing the lowest-energy open channel [see Fig. 1(a)]. This requires us to adiabatically track states between calculations performed at neighboring scattering lengths a_i and a_{i+1}, which can be uniquely followed by connecting states with the correct spin, inversion symmetry, and angular momentum L_z and the greatest wave function overlap $\langle\psi_m(a_i)|\psi_n(a_{i+1})\rangle$, where m and n are state indices.

II. DIRECT EXCHANGE

We first study two fermionic atoms trapped within the double-well potential. This is a minimal quantum simulator of the direct-exchange mechanism, exposes the competition between covalent and ionic bonding, and allows us to probe quantum entanglement. These three applications demand a thorough understanding of the exchange energy that we study with two complementary approaches: exact diagonalization and perturbation theory. The exchange energy can be probed directly in experiment by applying a magnetic field gradient and measuring the tunneling rate of atoms from the system [2,4]. The general interacting system with no central barrier has been studied by Busch *et al.* [6] so we first address a perturbative barrier before focusing on a high barrier.

Shallow barrier. We analyze the system analytically with first-order perturbation theory. For the $S = 0$ state we start with two opposite spin atoms in the Gaussian noninteracting ground state of the trapping potential with no central barrier $\phi_\sigma(\mathbf{r})$, and for $S = 1$ we start with two equal spin atoms with one excited into a state with a node either in the longitudinal or transverse directions depending on whether $\omega_\parallel$ or $\omega_\perp$ is smaller. Next we introduce the central barrier that within first-order perturbation theory induces a change in the energy of $\sum_\sigma \int d\mathbf{r}|\phi_\sigma(\mathbf{r})|^2 V_B \exp(-\omega_B z^2)$, and scattering that according to mean-field theory increases the energy by $4\pi a \int d\mathbf{r}|\phi_\uparrow(\mathbf{r})|^2|\phi_\downarrow(\mathbf{r})|^2$. This yields an exchange energy (energy difference between the $S = 0$ and $S = 1$ open channel states) of $-\Delta + oa/a_\parallel$ with $\Delta = \min(\omega_\parallel, \omega_\perp) - V_B\{[\omega_\parallel/(\omega_\parallel + \omega_B)]^{1/2} - [\omega_\parallel/(\omega_\parallel + \omega_B)]^{3/2}\}$, and overlap matrix element $o = \sqrt{2/\pi}\omega_\perp[1 - 4\sqrt{2}V_B/\pi(\omega_\parallel + \omega_B)]$. Increasing both the barrier height and interaction strength lowers the exchange energy. However, exact diagonalization confirms that the exchange energy is negative for any positive scattering length, so that a negative scattering length is required for an $S = 1$ ferromagnetic ground state in conformance with the Lieb-Mattis theorem [29].

High barrier. We now focus on a high barrier that presents a unique opportunity to study a minimal Hamiltonian of

localized spins. We initially exploit exact diagonalization to deliver the exact ground and excited states before developing an analytic theory to gain a heuristic understanding of the system. Finally, we demonstrate the versatility of the setup to study the competition between covalent and ionic bonding and quantum entanglement.

Results for a trap with $\omega_\parallel = \omega_\perp$ and a barrier with $V_B = 4\omega_\parallel$ are shown in Fig. 1(a). The exchange energy flips sign across unitarity, so that the red $S = 0$ level is the ground state for $a > 0$, and the blue $S = 1$ level for $a < 0$. On approaching unitarity from positive scattering lengths many molecular bands anticross the open channel from $0 \leqslant a_\parallel/a \lesssim 3$, removing the energy gap to the other states. Although the interaction potential harbors just one bound state, these bands correspond to the molecule being excited within the external trapping potential. Raising the central barrier increases the energy gap, presenting a larger range of the open channel to experiments. This should facilitate experiments that adiabatically transit across unitarity. Although the two-atom system cannot fall into a bound state without violating energy conservation, the closure of the energy gap precludes using this region to explore quantum entanglement. However, the super-Tonks regime is free from the molecular bands, making it the ideal venue to use the system as a quantum simulator and study quantum entanglement.

We next develop a complementary analytical expressions for the ground-state energy to gain an intuitive understanding of the system's behavior. We model the system by the Hubbard Hamiltonian $t\sum_\sigma(c_{L\sigma}^\dagger c_{R\sigma} + c_{R\sigma}^\dagger c_{L\sigma}) + \epsilon\sum_\sigma(c_{L\sigma}^\dagger c_{L\sigma} - c_{R\sigma}^\dagger c_{R\sigma}) + g(c_{L\uparrow}^\dagger c_{L\downarrow}^\dagger c_{L\downarrow} c_{L\uparrow} + c_{R\uparrow}^\dagger c_{R\downarrow}^\dagger c_{R\downarrow} c_{R\uparrow})$, where $c_{L\uparrow}^\dagger$ creates a particle localized in the left-hand well, $c_{R\uparrow}^\dagger$ creates a particle localized in the right-hand well, and ϵ denotes the relative depth of the wells. Diagonalization in the high-barrier limit $t \ll (\epsilon, go)$ yields an exchange energy of $-(1 + \epsilon^2 a_\parallel^2/16a^2o^2)t^2 a_\parallel/4ao$, where we use WKB perturbation theory [30] to derive the parameters $t = 32\omega_\parallel \exp(-2\sqrt{\pi V_B/\omega_B})/\pi^2$ and $o = 3\omega_\parallel\sqrt{\omega_\parallel}/(2\pi)^{3/2}$. We apply a magnetic field gradient dB/dz adding the term $\Delta H = \alpha z$ to the Hamiltonian, where $\alpha = g_J\mu_B dB/dz$ and g_J is the g factor. This gives a relative well depth of $\epsilon \simeq [\log(2\omega_B V_B/\omega_\parallel^2)/\omega_B]^{1/2}\alpha$. We find that the perturbative analysis matches well to the results of exact diagonalization around unitarity, as shown in Figs. 1(a) and 1(b).

Covalent versus ionic bonding. The covalent bonding in a crystal is driven by the negative exchange energy of electrons being shared between neighboring atoms. Conversely, in ionic bonding the constituent ions carry different electronegativities, driving a displacement of electron density that results in bond polarization and concomitant bonding. Cold atoms present an ideal simulator of the chemical bonding mechanisms, where the external potential portrays the atomic pseudopotential, the fermionic atoms represent the valence electrons, and the tilt ϵ represents the relative electronegativity tuning from $\epsilon = 0$ (covalent) to $|\epsilon| \sim \omega_\parallel$ (ionic character). Figure 1(b) shows that the exchange energy is $-(1 + \epsilon^2 a_\parallel^2/16a^2o^2)t^2 a_\parallel/4ao$, where in the absence of the tilt the first term $-t^2 a_\parallel/4ao$ corresponds to the covalent bonding, and the second term further lowers the energy in the presence of the tilt and so corresponds to the ionic contribution. On introducing the tilt

(a) Energy spectrum
(b) Tilted trap
(c) Qubit control protocol

(i) Prepare qubit in state $|\downarrow\uparrow\rangle$

(ii) Before evolution: qubit in state $|\downarrow\uparrow\rangle$

(iii) Evolve with interactions: singlet-triplet oscillation

(iv) After $t=\pi/E$: SWAP
Qubit in state $|\uparrow\downarrow\rangle$

(vi) After $t=2\pi/E$: identity
Qubit in state $|\downarrow\uparrow\rangle$

(v) Tilt to resolve and measure

(vii) Tilt to resolve and measure
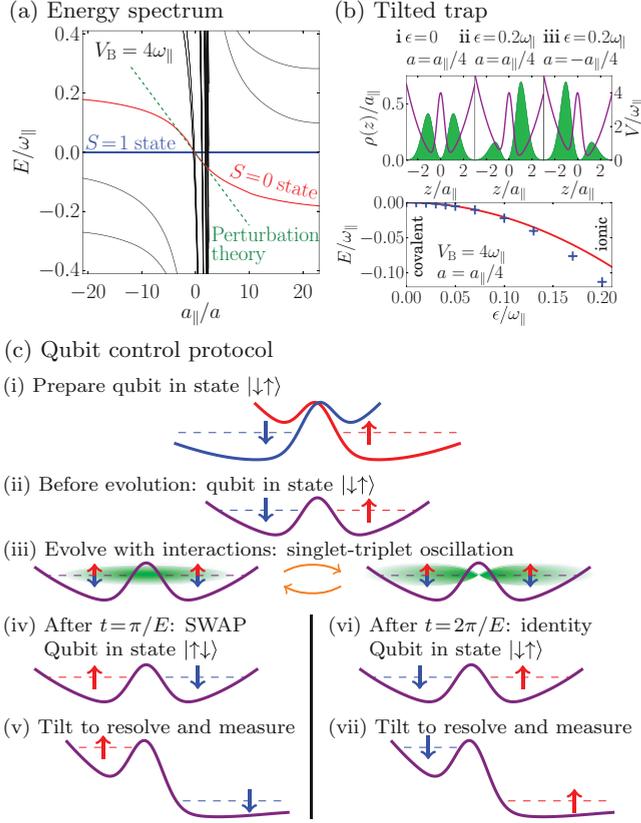
FIG. 1. (Color online) (a) Exchange energy from exact diagonalization (black lines), with the open channel (red line), the lowest $S=1$ state (blue line), and perturbation theory (green dashed line). (b) Bottom: Normalized exchange energy of the $S=0$ level as a function of relative well depth ϵ from exact diagonalization (blue crosses) and from the Hubbard Hamiltonian (red line). Top: The density profile (green) in the trap (magenta) at three values of the tilt and interaction strength. (c) Schematic of the experimental protocol to study quantum entanglement.

Fig. 1(b), i–ii demonstrates how the bond becomes polarized, with the increasing density in the lower well, $\sim a_\parallel^3 t^2 \epsilon/32 a^3 o^3$, lowering the net energy quadratically, $\sim\epsilon^2$, conforming with Pauling's definition of electronegativity [21,31]. The lowering of the energy and increasing polarization of the bond could be detected by tunneling atoms out of the two sides of the trap. Finally, Fig. 1(b), iii shows that with $a<0$ the atomic density would be counterintuitively pulled into the higher well.

Quantum entanglement. As the experimental setup offers a unique level of experimental control we are well positioned to explore quantum entanglement. The qubit control protocol is shown in Fig. 1(c). We define the first qubit state as the up-spin localized in the left-hand well and the down-spin localized in the right-hand well, denoted $|\downarrow\uparrow\rangle$ [Figs. 1(c), ii and 1(c), vi], and the second qubit state conversely, $|\uparrow\downarrow\rangle$ [Fig. 1(c), vi]. In Fig. 1(c), i the system is prepared into a qubit basis state in the noninteracting regime in the presence of a magnetic field gradient $g_J\mu_B dB/dz > t/a_\parallel$ in the Zeeman regime so that the two spins are driven in opposite directions [2]. With the configuration in Fig. 1(c), i we form the qubit state $|\downarrow\uparrow\rangle$ in

Fig. 1(c), ii. When the tilt is removed the qubit state $|\downarrow\uparrow\rangle$ is a superposition of the singlet and triplet states. With interactions the system will evolve under Rabi oscillations between the singlet and triplet states in Fig. 1(c), iii with a Rabi period $2\pi/E$, with $E = -t^2 a_\parallel/4ao$. A duration of π/E corresponds to a SWAP rotation [32] into the qubit state $|\uparrow\downarrow\rangle$ shown in Fig. 1(c), iv, and a duration of $2\pi/E$ corresponds to an identity rotation into the qubit state $|\downarrow\uparrow\rangle$ shown in Fig. 1(c), vi. To detect the qubit states in Figs. 1(c), v and 1(c), vii we apply a strong magnetic field gradient in the Paschen-Back regime to empty the right-hand well but leave the left-hand well occupied since it is shielded by the central barrier. The escaped atom carries a definite spin, resolving the system onto the qubit basis, and the remaining atomic spin can then be measured separately following the protocol in Ref. [2] to identify the qubit state. Finally, we note that $dE/d\epsilon|_{\epsilon=0}=0$ and therefore the Rabi period is insensitive to the controlling tilt parameter [33], making this an ideal opportunity to explore entanglement in a flexible, clean, and stable environment.

III. DOUBLE EXCHANGE

Two trapped atoms with a positive scattering length always yields an $S=0$ ground state [29]; so to realize the simplest possible ferromagnetic ground state we turn to a three-atom system. For a sufficiently strong central barrier this delivers a quantum simulator of the double-exchange mechanism for ferromagnetism: two atoms are localized in the lowest level of each well, and a third itinerant atom at a higher energy level couples their spins. With three atoms there are two possibilities for the highest occupied orbital: with either with a node longitudinally ($n_z=1$) or two degenerate modes with a transverse node ($n_{x,y}=1$). To study the emergence of magnetic correlations we use both exact diagonalization and perturbation theory. We adopt the same perturbation theory as introduced in the direct-exchange section for a small central barrier and weak scattering, except now for the three-atom states shown in Table I. To orient the discussion we focus initially on the realization of itinerant ferromagnetism before introducing a central barrier to consider the double-exchange mechanism.

Exact diagonalization delivers the phase diagrams in Fig. 2 that compare well with the perturbation theory predictions. At $V_B=0$ the system enters the $S=3/2$ state at $a/a_\parallel \approx 0.45$, which compares favorably to the perturbation calculation estimate that $a/a_\parallel = \sqrt{2/\pi}/3 \approx 0.84$ and a prediction that we extrapolated from the data of Liu of $a/a_\parallel \approx 1.1$ [8]. We note that the exact theory has a lower critical interaction strength than the perturbation theory prediction, which reflects the situation of the itinerant case [34,35]. The critical interaction strength is predicted to be independent of trap ellipticity $\omega_\perp/\omega_\parallel$ by both exact diagonalization and the perturbation theory calculations. In the high-barrier potential limit we follow the example from the direct-exchange calculation and model the system with the Hubbard Hamiltonian, predicting a crossover at $a/a_\parallel = \sqrt{\pi/2}/3 \approx 0.42$. This is in direct agreement with the results from exact diagonalization.

When $\omega_\parallel < \omega_\perp$ it is energetically favorable to occupy longitudinal modes and when $\omega_\parallel > \omega_\perp$ the transverse modes are preferred. However, the introduction of a central barrier favors longitudinal states ($n_z=1$) with a node across the barrier, with

TABLE I. Lowest-energy states for the three-atom system and their energy calculated in perturbation theory. Both the $S = 1/2$ and $S = 3/2$ states are shown, and also the available longitudinal and transverse modes.

Spin	State(s)	Orientation	Degeneracy	Energy
$S = \frac{1}{2}$	$c^\dagger_{000\downarrow} c^\dagger_{000\uparrow} c^\dagger_{001\uparrow}|0\rangle$	Longitudinal	1	$\frac{5}{2}\omega_\parallel + 3\omega_\perp + \sqrt{\frac{\omega_\parallel}{\omega_\parallel+\omega_B}} V_B \left(2 + \frac{\omega_\parallel}{\omega_\parallel+\omega_B}\right) + \frac{a}{a_\parallel}\omega_\perp\sqrt{\frac{2}{\pi}}\left(\frac{3}{2} - \frac{4\sqrt{2}}{\pi}\frac{V_B}{\omega_\parallel+\omega_B}\right)$
	$c^\dagger_{000\downarrow} c^\dagger_{000\uparrow} c^\dagger_{010\uparrow}|0\rangle$ $c^\dagger_{000\downarrow} c^\dagger_{000\uparrow} c^\dagger_{100\uparrow}|0\rangle$	Transverse	2	$\frac{3}{2}\omega_\parallel + 4\omega_\perp + 3\sqrt{\frac{\omega_\parallel}{\omega_\parallel+\omega_B}} V_B + \frac{a}{a_\parallel}\omega_\perp\sqrt{\frac{2}{\pi}}\left(\frac{3}{2} - \frac{6\sqrt{2}}{\pi}\frac{V_B}{\omega_\parallel+\omega_B}\right)$
$S = \frac{3}{2}$	$c^\dagger_{000\uparrow} c^\dagger_{001\uparrow} c^\dagger_{010\uparrow}|0\rangle$ $c^\dagger_{000\uparrow} c^\dagger_{001\uparrow} c^\dagger_{100\uparrow}|0\rangle$	Longitudinal	2	$\frac{5}{2}\omega_\parallel + 4\omega_\perp + \sqrt{\frac{\omega_\parallel}{\omega_\parallel+\omega_B}} V_B \left(2 + \frac{\omega_\parallel}{\omega_\parallel+\omega_B}\right)$
	$c^\dagger_{000\uparrow} c^\dagger_{010\uparrow} c^\dagger_{100\uparrow}|0\rangle$	Transverse	1	$\frac{3}{2}\omega_\parallel + 5\omega_\perp + 3\sqrt{\frac{\omega_\parallel}{\omega_\parallel+\omega_B}} V_B$

the crossover at $V_B = \sqrt{1 + \omega_B/\omega_\parallel}(1 + \omega_\parallel/\omega_B)(\omega_\parallel - \omega_\perp)$ for both $S = 1/2$ (at $a = 0$) and $S = 3/2$. A weak central barrier forces the atoms apart, reducing the effective interaction strength, meaning that the boundary between the $S = 1/2$ and $S = 3/2$ phases has a positive slope of $\sqrt{\omega_\parallel}(\omega_\parallel + \omega_\perp)/24\sqrt{\pi}$. With a larger central barrier the longitudinal $S = 1/2$ state and transverse $S = 3/2$ state share a phase boundary with a negative slope giving rise to a characteristic notch.

The phases are distinguished not only by their spin quantum number but also by the degeneracy associated with the orientation of the node in the highest occupied orbital. The changing degeneracy means that the phases with the same spin quantum number cannot evolve into one another so there is a quantum phase transition between the two. In a cold-atom gas both total spin and symmetry are conserved, so to probe the phase diagram a tunneling measurement is proposed [2], with

FIG. 2. (Color online) The phase diagrams predicted by exact diagonalization (left) and perturbation theory (right) at three different trap ratios. The phase corresponding to the each color is identified in each diagram, with "L" indicating a longitudinal phase and "T" a transverse phase. The arrows show the critical interaction strength predicted by the Hubbard model.

the gas starting from four atoms, tilting the trap, and tunneling down to the three-atom configuration with the lowest energy. At the critical interaction strength the $S = 1/2$ and $S = 3/2$ states will be formed with equal likelihood, but taking account of the degeneracy will boost the formation of the doubly degenerate states, presenting an ideal tool to characterize the phases.

The high-barrier perturbation theory provided a perfect description for the phase behavior predicted by exact diagonalization theory in that limit. This demonstrates that the ferromagnetism is driven by double exchange, consistent with the observed exponential decay of the interaction matrix element between one atom localized in the left-hand well and another localized in the right-hand well. However, the high-barrier perturbation theory is unable to describe the system with a low central barrier, where the requirement to have orbitals with a longitudinal node is incompatible with the nodeless "transverse" wave functions found in exact diagonalization and shown in Table I, which are of itinerant nature. Therefore, the crossover from "transverse" to "longitudinal" wave functions in the phase diagram denotes the underlying ferromagnetic correlations changing from itinerant to localized double exchange.

IV. DISCUSSION

The double well system is the perfect playground to study the exchange mechanisms of strongly interacting fermions. We have studied the direct exchange mechanism that is the fundamental building block of Heisenberg antiferromagnetism and exposes the competition between covalent and ionic bonding. The experimental flexibility of the cold atom gas also presents the ideal arena to study quantum entanglement. Trapping three fermions delivers the first faithful realization of the double exchange mechanism. This can provide insights into Heisenberg ferromagnets and 90° superexchange, and be built up to larger lattices through a cluster expansion.

The exchange mechanisms presented here give a tantalizing insight into the broad range of effects that can be explored in the double well potential. The inclusion of a third potential well would allow investigators to study the Kramers-Anderson superexchange mechanism [36] behind many antiferromagnets. Trapping more atoms should reveal an even/odd effect of flipping between antiferromagnetic and ferromagnetic ground states.

[1] P. Cheinet, S. Trotzky, M. Feld, U. Schnorrberger, M. Moreno-Cardoner, S. Fölling, and I. Bloch, Phys. Rev. Lett. **101**, 090404 (2008).

[2] F. Serwane, G. Zürn, T. Lompe, T. B. Ottenstein, A. N. Wenz, and S. Jochim, Science **332**, 336 (2011)

[3] G. Zürn, F. Serwane, T. Lompe, A. N. Wenz, M. G. Ries, J. E. Bohn, and S. Jochim, Phys. Rev. Lett **108**, 075303 (2012).

[4] M. Rontani, Phys. Rev. Lett. **108**, 115302 (2012).

[5] Z. Idziaszek and T. Calarco, Phys. Rev. A **74**, 022712 (2006).

[6] T. Busch, B.-G. Englert, K. Rzążewski, and M. Wilkens, Found. Phys. **28**, 549 (1998).

[7] C. Mora, R. Egger, A. O. Gogolin, and A. Komnik, Phys. Rev. Lett. **93**, 170403 (2004).

[8] X.-J. Liu, H. Hu, and P. D. Drummond, Phys. Rev. A **82**, 023619 (2010).

[9] D. Rubeni, A. Foerster, and I. Roditi, Phys. Rev. A **86**, 043619 (2012).

[10] S. E. Gharashi, K. M. Daily, and D. Blume, Phys. Rev. A **86**, 042702 (2012).

[11] I. Brouzos and P. Schmelcher, Phys. Rev. A **87**, 023605 (2013).

[12] E. C. Stoner, Proc. R. Soc. London, Ser. A **165**, 372 (1938).

[13] P. O. Bugnion and G. J. Conduit, Phys. Rev. A **87**, 060502(R) (2013).

[14] G. Burkard, D. Loss, and D. P. DiVincenzo, Phys. Rev. B **59**, 2070 (1999).

[15] E. A. Laird, J. R. Petta, A. C. Johnson, C. M. Marcus, A. Yacoby, M. P. Hanson, and A. C. Gossard, Phys. Rev. Lett. **97**, 056801 (2006).

[16] L.-X. Zhang, D. V. Melnikov, and J.-P. Leburton, J. Phys.: Condens. Matter **21**, 095502 (2009).

[17] J. R. Petta, A. C. Johnson, J. M. Taylor, E. A. Laird, A. Yacoby, M. D. Lukin, C. M. Marcus, M. P. Hanson, and A. C. Gossard, Science **309**, 2180 (2005).

[18] S. Trotzky, P. Cheinet, S. Fölling, M. Feld, U. Schnorrberger, A. M. Rey, A. Polkovnikov, E. A. Demler, M. D. Lukin, and I. Bloch, Science **319**, 295 (2008).

[19] D. Greif, T. Uehlinger, G. Jotzu, L. Tarruell, and T. Esslinger, Science **340**, 6138 (2013).

[20] M. G. Raizen, S.-P. Wan, C. Zhang, and Q. Niu, Phys. Rev. A **80**, 030302(R) (2009).

[21] G. Barrow, J. Chem. Phys. **26**, 558 (1957).

[22] D. Hayes, P. S. Julienne, and I. H. Deutsch, Phys. Rev. Lett. **98**, 070501 (2007).

[23] C. J. Foot and M. D. Shotter, Am. J. Phys. **79**, 762 (2011).

[24] X.-J. Liu, H. Hu, and P. D. Drummond, Phys. Rev. Lett. **102**, 160401 (2009).

[25] S. Nascimbène, N. Navon, K. Jiang, F. Chevy, and C. Salomon, Nature (London) **463**, 1057 (2010).

[26] A. Szabó and N. S. Ostlund, *Modern Quantum Chemistry: Introduction to Advanced Electronic Structure Theory* (Dover, New York, 1989).

[27] T. Helgaker, P. Jørgensen, and J. Olsen, *Molecular Electronic Structure Theory* (Wiley & Sons, New York, 2000).

[28] I. S. Gradshteyn and I. M. Ryzhik, *Table of Integrals, Series, and Products* (Elsevier/Academic Press, Amsterdam, 2007).

[29] E. Lieb and D. Mattis, Phys. Rev. **125**, 164 (1962).

[30] E. L. Platt, Thesis, University of Waterloo, 2008.

[31] L. Pauling, *The Nature of the Chemical Bond* (Cornell University Press, Ithaca, NY, 1945).

[32] M. A. Nielsen and I. L. Chuang, *Quantum Computation and Quantum Information* (Cambridge University Press, Cambridge, UK, 2000).

[33] M. Stopa and C. M. Marcus, Nano Lett. **8**, 1778 (2008).

[34] G. J. Conduit and B. D. Simons, Phys. Rev. A **79**, 053606 (2009).

[35] G. J. Conduit, A. G. Green, and B. D. Simons, Phys. Rev. Lett. **103**, 207201 (2009).

[36] P. W. Anderson, Phys. Rev. **79**, 350 (1950).